ACS APPLIED ENERGY MATERIALS

www.acsaem.org Article

8.0% Efficient Submicron $CuIn(S,Se)_2$ Solar Cells on $Sn:In_2O_3$ Back Contact via a Facile Solution Process

Yao Gao, Guanchao Yin,* Yong Li, Tristan Köhler, Jan Lucaßen, and Martina Schmid*

Cite This: *ACS Appl. Energy Mater.* 2022, 5, 12252−12260 Read Online

ACCESS | Metrics & More | Article Recommendations | Supporting Information

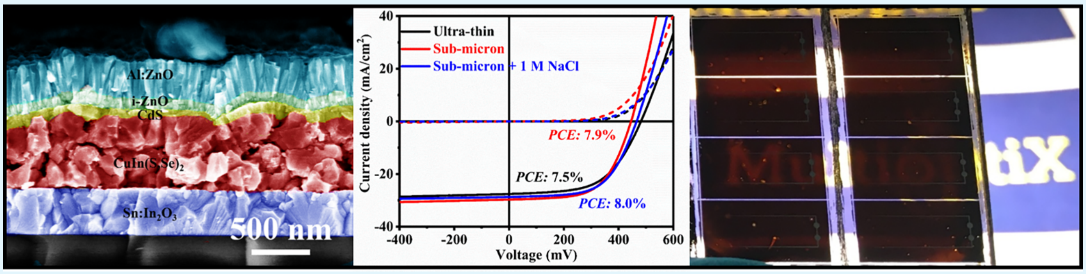

ABSTRACT: High-performance chalcopyrite solar cells have been fabricated on transparent conductive oxide (TCO) back contact through an environmentally benign solution, showing great potential for bifacial application. Ultrathin (around 550 nm) $CuIn(S,Se)_2$ (CISSe) solar cells were successfully deposited on $Sn:In_2O_3$ (ITO) back contact via spin-coating of metal-chloride *N,N*-dimethylformamide (DMF) solution, followed by selenization. The ultrathin devices achieved a conversion efficiency of 7.5% when the precursor film was selenized at 520 °C. With the increase in the absorber thickness to submicron (740 nm), the solar cells exhibited not only a higher short-circuit current density but also an improved fill factor compared to the ultrathin devices, which resulted in an efficiency enhancement to 7.9%. Furthermore, NaCl solution preselenization treatment was demonstrated to improve the performance of CISSe solar cells. When the submicron absorber was subject to 1 M NaCl solution prior to selenization, an 8.0% efficient CISSe device was achieved. To the best of our knowledge, this is the topmost performance for submicron CISSe solar cells fabricated from solution-based precursors on TCO back contact.

KEYWORDS: *CISSe solar cells, submicron absorber, ITO back contact, spin-coating, solution processing, NaCl preselenization treatment*

1. INTRODUCTION

Photovoltaics is considered one of the most promising energy-harvesting technologies because it can directly convert the basically unlimited resource of solar energy to electrical energy. Copper indium gallium diselenide-based (CIGSe-based) solar cells with a champion efficiency of 23.35% were achieved with a 2−3 μm thick absorber layer.[1] However, the thick CIGSe absorber relates to high cost, for example, due to the large consumption of scarce elements (In and Ga). Therefore, thinning the absorber layer would be conducive to reducing the absorber deposition duration and lessening the usage of scarce elements, simultaneously increasing production throughput and reducing manufacturing costs.[2−7]

Generally, molybdenum (Mo) is employed as a back contact for high-efficiency CIGSe solar cells because a $MoSe_2$ interlayer between Mo back contact and CIGSe absorber will form during the absorber growth process and lead to a quasi-Ohmic contact.[8] However, due to the poor back reflectivity of the CISSe/Mo interface, ultrathin (around 500 nm) CIGSe solar cells suffer from dramatic optical losses. In addition, the opacity of the Mo back contact limits their application in bifacial and semitransparent structures.[9] Therefore, replacing opaque Mo with a transparent conductive oxide (TCO) as back contact is promising. In previous reports, Al:ZnO (AZO), $F:In_2O_3$ (FTO), and $Sn:In_2O_3$ (ITO) have been used to replace the Mo back contact of CIGSe solar cells fabricated via a coevaporation process.[5,7,10,11] However, coevaporation deposition is an expensive fabrication technique requiring a high-vacuum environment. Therefore, the exploitation of a cost-effective and convenient process for CIGSe solar cell fabrication is crucial.

In past decades, the solution-based process has been proven a promising technique for chalcopyrite solar cell growth. The champion photovoltaic conversion efficiency (*PCE*) of $Cu(In,Ga)(S,Se)_2$ (CIGSSe) solar cells fabricated by a hydrazine-based solution process is 18.1%.[12] However, hydrazine is a highly toxic solution, which prohibits its industrial production for health, environmental, and safety concerns. Jiang et al. have

Received: June 6, 2022
Accepted: September 8, 2022
Published: September 23, 2022

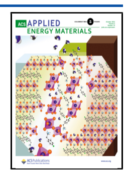

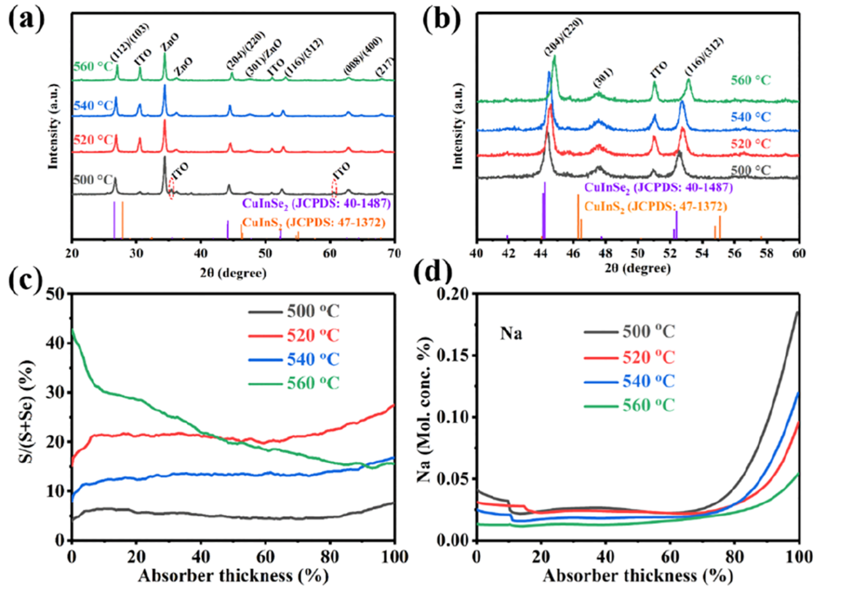

Figure 1. (a,b) XRD pattern of the CISSe solar cell devices selenized at different temperatures and (c) S/(S + Se) ratios and (d) Na content of the absorber layers measured by GDOES.

proven *PCE*s of 14.5% for CISSe and 15.2% for CIGSSe solar cells with 1.2 μm absorbers. These were obtained via a solution-based spin-coating process with metal chloride-DMF (DMF: *N*,*N*-dimethylformamide) precursor ink, indicating that metal-chloride DMF as a precursor solution shows high potential in CIGSe-based solar cell fabrication.[13−15] A CIGSe device with an efficiency of 13.8% was achieved successfully via an all-solution-processed fabrication (except for the Mo back contact).[16] On ITO back contact, Barange et al. reported 5.68% efficiency for CIGS via a spin-coating process of sol−gel solution.[17] Sousa et al. reported 6.1% efficiency for CIGSe on FTO back contact via a screen-printing process.[18] However, the solar cell properties exhibited poor homogeneity.

Here, we first demonstrate 7.5% efficiency for ultrathin CISSe solar cells (550 nm absorber) deposited on ITO back contact from metal-chloride DMF solution, which is the highest efficiency of ultrathin CISSe solar cells fabricated on TCO back contact via a solution process. We find that the selenization temperature is a key for achieving high crystallinity, morphology, and homogeneity of the CISSe absorbers. To improve the efficiency of the CISSe solar cells, three different thicknesses (550, 740, and 1440 nm CISSe) of the absorber layer are investigated. The absorbers with thicknesses of 550, 740, and 1400 nm are referred to as ultrathin, submicron, and micron absorbers, respectively. A corresponding terminology is used for the related CISSe solar cells. The submicron CISSe solar cells show the best photovoltaic properties. The efficiency of the CISSe solar cells with a 740 nm absorber is further improved after being subject to a preselenization treatment with 1 M NaCl solution. 8.0% *PCE* is achieved for submicron CISSe solar cells with NaCl solution preselenization treatment, which is the topmost efficiency for submicron CISSe solar cells fabricated from solution-based precursors on TCO back contact. These high-quality submicron CISSe solar cells show great potential for bifacial applications.

2. EXPERIMENTAL SECTION

2.1. ITO Back Contact Deposition. ITO back contacts of 400 nm thickness were deposited on soda-lime glass substrate by DC-sputtering in a PRO Line PVD 75 (Kurt J. Lesker Company). It was reported that the electrical and optical performance of the ITO back contact can be improved by annealing.[19] The ITO back contacts are subject to an annealing treatment at 350 °C for 10 min in air before spin-coating the precursor solution. The sheet resistances and optical properties are shown in Figure S1. Sheet resistances of ITO without and with annealing are quite comparable. Pre-annealing treatment improves the transmission in the wavelength range from 300 to 600 nm and increases absorption from 500 to 1200 nm. The pre-annealing process can improve the wetting property between ITO and precursor solution, which is favorable for the formation of a flat film.

2.2. Fabrication of CISSe Solar Cells. For the CuCl-$InCl_3$-thiourea (TU) solution, 1.197 g of TU (99%, Alfa Aesar) were first added to 8 mL of DMF (99.8%, Sigma-Aldrich) solvent to form a clear solution after 20 min stirring. Then, 0.253 g of CuCl (99.8%, Sigma-Aldrich) were added to this solution and stirred until CuCl completely dissolved. Finally, 0.608 g of $InCl_3$ (99.8%, Sigma-Aldrich) were added and a yellowish solution was obtained after overnight stirring. The solution was filtered by using a 0.45 μm polytetrafluoroethylene filter before spin-coating. To improve the wetting property of the ITO back contacts with the precursor solution, the ITO back contacts were annealed at 350 °C for 10 min before spin-coating. The solution was deposited on ITO back contacts via spin-coating at 1500 rpm for 60 s. Then, the films were immediately annealed on a hot plate at 350 °C for 2 min and moved to a ceramic plate for cooling down naturally. The coating−annealing−cooling cycle was repeated 5 times, 8 times, and 15 times to make total film thicknesses of around 550 nm (ultrathin), 740 nm (submicron), and 1440 nm (micron), respectively. The as-prepared Cu-In-S precursor films were placed into a tube furnace with an Ar atmosphere and 250 mg Se powder. They were then subject to a first heating step at 350 °C for 15 min and a second step at an enhanced temperature for 20 min to form CISSe thin films. For the preselenization sodium treatment, the as-prepared submicron Cu-In-S precursor films were soaked in 0.4, 0.8, or 1 M NaCl aqueous-ethanol solution (the volume ratio of water to ethanol is 1:1) for 10 min, respectively.[20] After selenization, the as-annealed films were etched in a 10% KCN solution for the removal of Cu_{2-x}(S,Se). Then, an 80 nm CdS buffer layer was deposited onto the CISSe thin films by chemical bath deposition, and an 80 nm *i*-ZnO/300 nm AZO bilayer was sputtered successively. A Ni/Al top grid was deposited by thermal evaporation. The active area of each CISSe solar cell was 0.5 cm^2 defined by mechanical scribing.

2.3. Characterization. Grazing-incidence X-ray diffraction (GIXRD) with an incidence angle of 0.5° was used to obtain the structure of the as-prepared films. The data was collected employing an X'Pert PRO diffractometer (PANalytical) with Ni-filtered Cu Kα radiation and a PIXcel detector. The morphology of the photovoltaic devices was obtained by LEO 1500 scanning electron microscopy (SEM). The composition of the CISSe absorbers was extracted by calibrated energy-dispersive X-ray fluorescence of type SPECTRO XEPOS. The elemental profiles of the absorbers were identified by glow discharge optical emission spectroscopy (GDOES) on the instrument SPECTRO XEPOS. The current density−voltage ($J-V$) curves were measured under standard test conditions (AM1.5; 100 mW/cm^2; 25 °C) by a WACOM sun-simulator containing both a xenon and a halogen lamp. The external quantum efficiency (EQE) was measured on a home-built system applying calibrated Si and Ge diodes as references. In addition, the capacitance−voltage ($C-V$) curves were obtained under dark conditions with a BK PRECISION Model 895 operating at 100 kHz and a 5 mV testing signal.

3. RESULTS

3.1. Effect of Selenization Temperature. Figure 1a shows the GIXRD patterns of ultrathin CISSe thin-film solar cells. The positions of Bragg reflections at 26.9, 44.7, and 53.1° correspond to the (112)/(103), (204)/(220), and (116)/(312) planes of chalcopyrite, respectively.[13] Since the radius of the selenium atom is larger than that of sulfur, the positions of these Bragg reflections are right-shifted compared to pure $CuInSe_2$ and left-shifted compared to pure $CuInS_2$. Bragg reflections located at 30.5 and 50.9° are attributed to the ITO back contact. Additionally, the Bragg reflections pointing to the ZnO window layer are observed at 34.4, 36.2, and 47.6°. When the selenization is carried out at T = 500 °C, additional Bragg reflections of ITO at 35.4 and 60.7° appear. Compared to T = 500 °C, the XRD diffraction patterns for absorbers selenized at $T \geq 520$ °C show a slight right shift (Figure 1b), especially at high diffraction angles where the shift of the Bragg reflections is more pronounced. This result indicates that as-prepared absorber layers at $T \geq 520$ °C have a higher S/(S + Se) ratio, which is confirmed by XRF measurements, as shown in Table S1.[21] However, for the CISSe absorber obtained at 540 °C, the shift of XRD patterns is not as obvious as for the absorbers at 520 and 560 °C. This observation is also in agreement with a lower S/(S + Se) ratio, see Table S1.

The S/(S + Se) depth profiles of the CISSe absorbers are measured via GDOES and are shown in Figure 1c. With the increase of the selenization temperature above 500 °C, the content of S increases. It indicates that in the process of selenization at higher temperatures, the higher Se pressure suppresses the evaporation of S, accordingly inhibiting the replacement of Se by S. When $T \leq 540$ °C, the S content at the CISSe back interface is higher than at the front interface. In addition, when T = 540 °C, the content of S is lower than that for T = 520 °C and T = 560 °C, which is in agreement with the position of the XRD peaks (Figure 1b). However, when increase the temperature to T = 560 °C, the opposite dependency is observed regarding the S/(S + Se) ratio. There is a factor of two higher S content at the front compared to the back interface. This observation may be explained by large grains in the CISSe layer forming rapidly under high Se pressure at high temperatures. However, S will volatilize along the grain boundary of this large-grain layer, leading to inhomogeneous grains at the front interface of the CISSe absorber (Figure 2d). The near front surface consists of large CISSe grains and an aggregation of small CISSe grains. Large CISSe grains form at the rear interface of the CISSe absorber. In general, the grain size of CISSe with a Se-rich composition is larger than for S-rich CISSe.[8] Therefore, a higher S/(S + Se) ratio is observed at the front surface and decreases toward the rear interface. The GDOES results are in good agreement with XRD and XRF measurements (Table S1). Na exhibits a similar trend in these solar cells (Figure 1d). A high Na content exists near the back interface, and then it decreases toward the front surface. A high selenization temperature can promote the diffusion of Na from the substrate to the absorber layer. However, with increasing selenization temperature, the Na content of the absorber decreases in our experiments (Figure 1d). The reason may be a removal of Na near the surface during the KCN etching and the CdS deposition process. Na can stay at the grain boundary and grain interior.[22] The higher Na content for 500 °C selenization temperature is attributed to its significantly smaller grains and higher density of grain boundaries.[13]

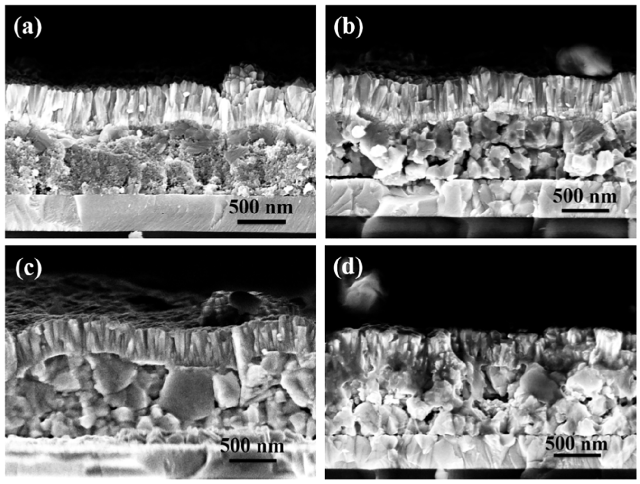

Figure 2. SEM images of CISSe solar cells prepared at different selenization temperatures: (a) 500, (b) 520, (c) 540, and (d) 560 °C.

The cross-sectional SEM images of the CISSe devices with varied selenization temperatures are shown in Figure 2. For T = 500 °C, the CISSe absorber shows a double-layer structure with a thick sublayer of fine grains at the bottom and a very thin sublayer with large grains on top, implying that the low selenization temperature is disadvantageous to CISSe grain growth. When the selenization temperature increases to T = 520 °C, larger grains of around 300−500 nm size are observed. However, voids still exist in the absorber layer and at the back contact interface. The largest CISSe grains with diameters of around 500−650 nm form when the precursor film selenization is carried out at 540 °C. In this case, the large grains of the absorber layer are densely packed, almost absent of voids. When the selenization temperature increases to 560 °C, a CISSe absorber layer with a triple-layer structure is observed: large grains at the bottom and on top and fine grains in the middle. However, the top layer consists of large CISSe grains and an aggregation of small CISSe grains (Figure 2d, left: fine grain aggregation; right: large grains). This inhomogeneous morphology can be ascribed to the difference in elemental distribution. A large amount of liquid Se penetrates the whole film under high Se vapor pressure, and Se bonds with Cu to form $Cu_{2-x}Se$, which facilitates the formation of large grains and denser films.[13,23] However, S

https://doi.org/10.1021/acsaem.2c01764
ACS Appl. Energy Mater. 2022, 5, 12252−12260

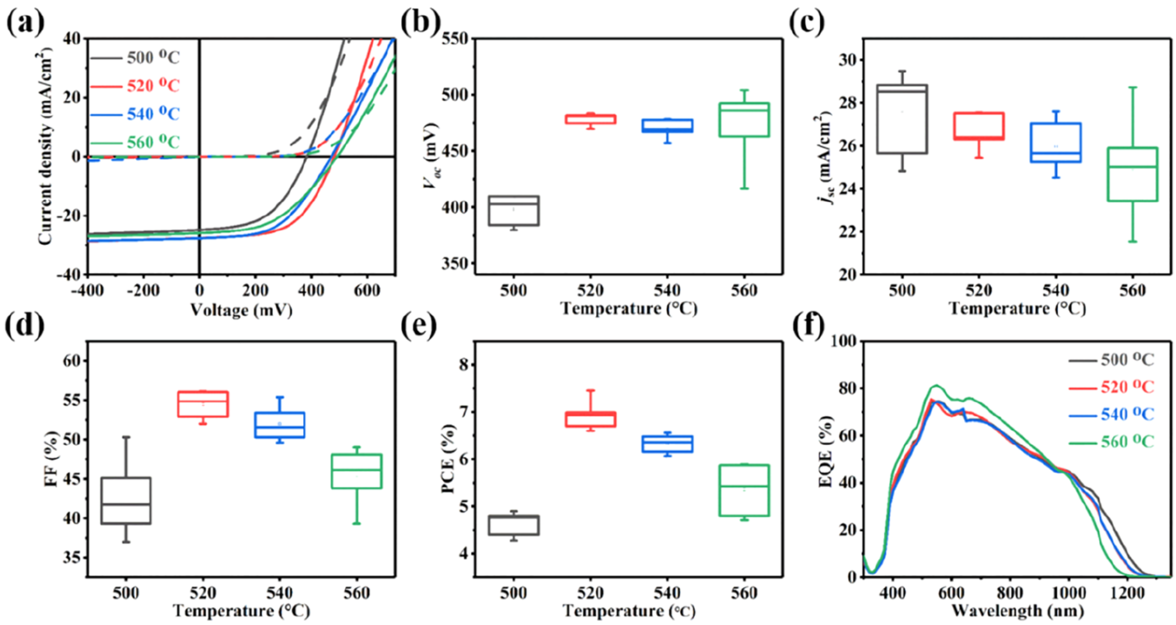

Figure 3. (a) $J-V$ curves of the best CISSe devices grown on ITO back contact at various selenization temperatures. The distribution (each sample contained six cells) of (b) open-circuit voltage (V_{oc}), (c) short-circuit current (j_{sc}), (d) *FF*, and (e) *PCE*. (f) EQE of the best CISSe devices.

Table 1. Photovoltaic Parameters Averaged over Six CISSe Devices and for the Highest-Efficient CISSe Device Grown on ITO Back Contact at Various Selenization Temperatures (Corresponding to Figure 3)

selenization temperature	V_{oc} (mV)	j_{sc} (mA/cm²)	*FF* (%)	*PCE* (%)	R_s (Ω cm²)
500 °C	398.1 ± 13.1	27.6 ± 1.9	42.5 ± 4.7	4.7 ± 0.2	
	384.1	24.8	50.3	4.8	1.7
520 °C	478.6 ± 5.3	26.6 ± 0.8	54.5 ± 1.7	6.9 ± 0.3	
	481.7	27.6	56.1	7.5	2.2
540 °C	469.8 ± 7.9	26.0 ± 1.2	52.0 ± 2.2	6.3 ± 0.2	
	471.7	27.6	50.3	6.6	4.3
560 °C	474.6 ± 31.6	24.9 ± 2.5	45.4 ± 3.5	5.4 ± 0.6	
	492.2	25.9	46.1	5.9	5.8

tends to stronger volatilize when the precursor films are selenized at 560 °C. Additionally, the as-formed dense large grains will inhibit the S outflow (Figure 2d).[23] Sulfur can only evaporate in the area containing abundant grain boundaries, leading to the formation of S-rich CISSe grains with small grain size after selenization. Even though large grains are located at both the bottom and top of the absorber, the grain size of the bottom layer is more homogeneous than that of the top one. A possible reason is that bottom CISSe grains have a high content of Se and a more homogeneous elemental composition than CISSe grains on top of the absorber (Figure 1c).

Figure 3a shows the $J-V$ curves of the best CISSe solar cells under AM 1.5G illumination, and the corresponding photovoltaic parameters are summarized in Table 1. When the selenization is carried out at T = 500 °C, a maximum *PCE* of 4.8% is achieved with a short-circuit current density (j_{sc}) of 24.8 mA/cm², an open-circuit voltage (V_{oc}) of 384.1 mV, and a fill factor (*FF*) of 50.3%. The *PCE* at T = 520 °C is remarkably enhanced to 7.5%. The efficiency improvement can be explained by the better crystallinity at high temperatures. However, when the selenization temperature increases to T = 540 °C and T = 560 °C, the *PCE*s decrease to 6.6, and 5.9%, respectively. The same trend can be observed in j_{sc} and *FF*; the highest j_{sc} of 27.6 mA/cm² and *FF* of 56.1% are obtained at 520 °C. However, the highest V_{oc} value of 492.2 mV is achieved when the temperature increases to 560 °C. The higher V_{oc} can be attributed to the better crystallinity and the higher content of S observed at higher selenization temperatures. Simultaneously, due to the wider band gap of the CISSe absorber with higher S content, j_{sc} is lowered.[8,12] The series resistance (R_s) values of the samples are calculated from the plots of dV/dJ versus $1/(J + J_{sc})^1$ (shown in Figure S3). With increasing selenization temperature, R_s increases from 1.7 Ω cm² (for 500 °C) to 2.2 Ω cm² (for 520 °C), 4.3 Ω cm² (for 540 °C), and 5.8 Ω cm² (for 560 °C), respectively. The enhancement of R_s with increasing absorber selenization temperature ascribes to the formation of a thin In_2O_3 layer at the CISSe/ITO interface during the high-temperature selenization owing to the low standard molar enthalpy of In_2O_3.[24]

As shown in Figure 3b, the V_{oc} values of the solar cells increase with increasing selenization temperature. However, when the precursor films are selenized at T = 540 °C, the V_{oc} values of the corresponding solar cells slightly decrease. This variation tendency of V_{oc} can be related to the content of S in the CISSe absorbers (Table S1). Increasing the selenization temperature results in a decrease of j_{sc} (Figure 3c) because the CISSe absorber has a wider band gap for high selenization temperature due to the increase of S content (Table S1). Both *FF* and *PCE* increase with increasing selenization temperature to T = 520 °C and then decrease with further rise of the

https://doi.org/10.1021/acsaem.2c01764
ACS Appl. Energy Mater. 2022, 5, 12252−12260

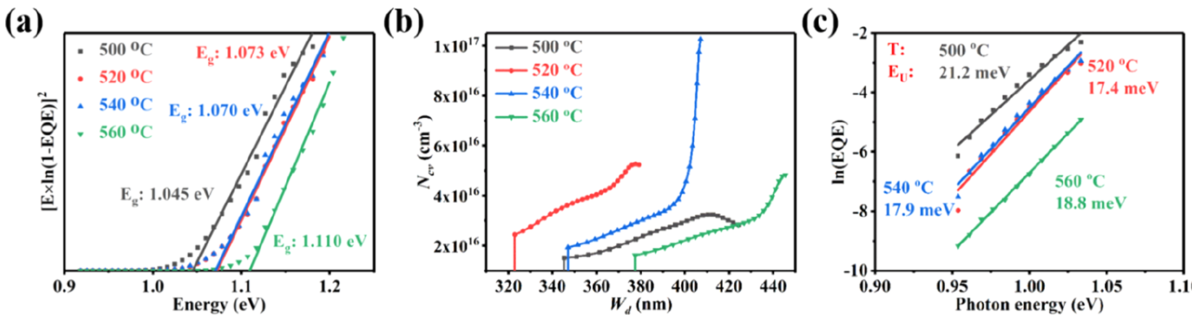

Figure 4. (a) Band gaps of devices with different selenization temperatures calculated from EQE data. (b) Charge carrier density and depletion width derived from C−V curves. (c) ln(EQE) vs photon energy at the long-wavelength edge to determine the E_U values for CISSe devices with different selenization temperatures.

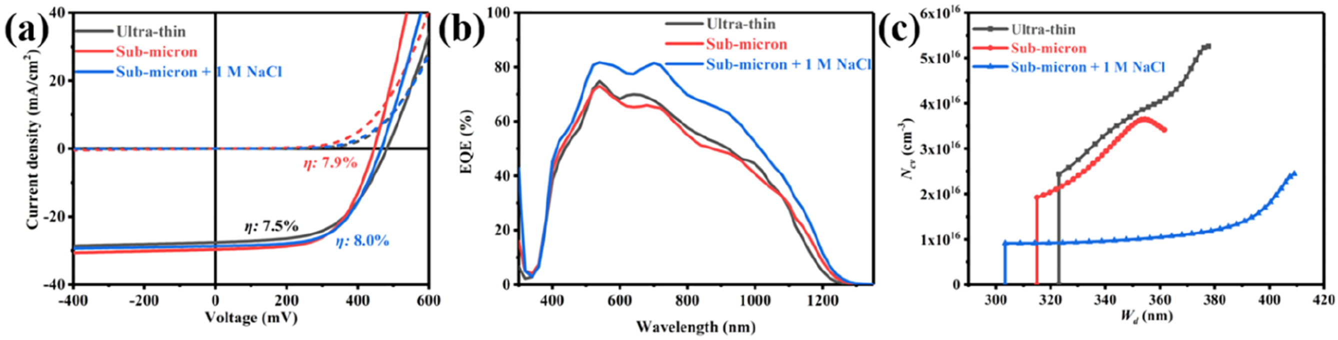

Figure 5. (a) J−V, (b) EQE curves, and (c) N_{cv}-W_d relation of the best CISSe devices with different absorber thicknesses and with NaCl treatment grown on ITO back contact.

selenization temperature (Figure 3d,e). These results indicate that T = 520 °C is favorable for fabricating high-quality CISSe absorbers on ITO back contact for semitransparent CISSe solar cell applications.

The EQE spectra of the best devices are shown in Figure 3f and the optical properties are shown in Figure S2. These EQEs are higher than 65% in the visible wavelength range, and the intensity of the EQE response surpasses 75%. However, the EQE results are relatively low because of the thin absorber layer (550 nm). The device applying the absorber selenized at T = 560 °C shows a higher EQE in the range from 380 to 950 nm wavelength compared to the samples of other annealing temperatures. However, the EQE drops rapidly when the wavelength is longer than 1000 nm owing to a higher content of S in the absorber selenized at T = 560 °C compared to those selenized at T < 560 °C (Table S1). The EQE spectra of all devices are overlapping in the range of 300−380 nm wavelength owing to the absorption originating from the CdS/i-ZnO/AZO layers.[7]

From the EQE spectra of the devices with the highest efficiency, band gaps can be calculated (see Figure 4a). The band gaps of these CISSe devices extracted from the $[E \times \ln(1 - \mathrm{EQE})]^2$ versus energy plots are shown in Figure 4a. With increasing selenization temperature, wider band gaps are observed. When T = 500 °C, a 1.04 eV band gap is obtained. With the increase of the selenization temperature to T = 520 °C and T = 540 °C, similar band gap values (1.07 eV for 520 °C and 1.08 eV for 540 °C) are observed from EQE calculation results. The absorber carrying out selenization at T = 560 °C shows the widest band gap of 1.11 eV. These results are in good agreement with the V_{oc} improvement at higher selenization temperatures as compared to T = 500 °C.

The profiles of carrier concentration (N_{cv}) versus depletion width (W_d) are calculated from $C - V$ curves (Figure 4b).[7] N_{cv} of 1.5 × 10^{16} and W_d of 345.3 nm are obtained when the CISSe absorber is selenized at 500 °C. When the selenization temperature increases to 520 °C, N_{cv} increases to 2.3 × 10^{16} cm^{-3} and W_d thus decreases to 323.1 nm, respectively. However, with further increasing selenization temperature, N_{cv} decreases from 2.3 × 10^{16} cm^{-3} (T = 520 °C) to 1.9 × 10^{16} cm^{-3} (T = 540 °C) and 1.6 × 10^{16} cm^{-3} (T = 560 °C). Correspondingly, W_d increases from 323.1 nm (T = 520 °C) to 347.1 nm (T = 540 °C) and 377.5 nm (T = 560 °C), respectively. It is reported that the high-quality CIGSe solar cells have a high carrier concentration and a related narrow depletion width.[25,26] As a result, the highest values of performance parameters are obtained for devices selenized at 520 °C.

Figure 4c shows the relation of ln(EQE) versus photon energy at the long wavelength edge (1200−1300 nm). From this, the Urbach energy (E_U) can be extracted, which affects the carrier mobility and lifetime of the solar cells.[27,28] E_U decreases from 20.2 meV (T = 500 °C) to 17.4 meV (T = 520 °C) with a related increase in *PCE* from 4.8 to 7.5% because the enlargement of CISSe grain size is obtained at T = 520 °C, leading to good absorber quality.[28] However, when the selenization temperature continues to increase, E_U increases to 17.9 meV (T = 540 °C, η = 6.6%) and 18.8 meV (T = 560 °C, η = 5.9%), respectively. It indicates that an even higher temperature is not beneficial for preparing high-efficiency CISSe solar cells on ITO back contact. Conclusively, the best solar cell properties are achieved for selenization at T = 520 °C. Therefore, this temperature is used for further research in this work.

https://doi.org/10.1021/acsaem.2c01764
ACS Appl. Energy Mater. 2022, 5, 12252−12260

Table 2. Averaged (over Six Devices) and Best CISSe Photovoltaic Device Parameters for Ultrathin CISSe, Submicron CISSe, and Submicron CISSe Implementing 1 M NaCl Solution Treatment

	V_{oc} (mV)	j_{sc} (mA/cm^2)	FF (%)	PCE (%)	R_s (Ω cm^2)
ultra-thin CISSe	478.6 ± 5.3	26.6 ± 0.8	54.5 ± 1.7	6.9 ± 0.3	
	481.7	27.6	56.1	7.5	2.2
sub-micron CISSe	448.5 ± 2.6	29.1 ± 0.6	56.3 ± 3.2	7.3 ± 0.4	
	445.6	29.7	59.8	7.9	1.1
sub-micron CISSe + 1 M NaCl	463.9 ± 5.9	28.2 ± 0.6	58.0 ± 2.0	7.6 ± 0.3	
	466.0	28.7	59.6	8.0	1.7

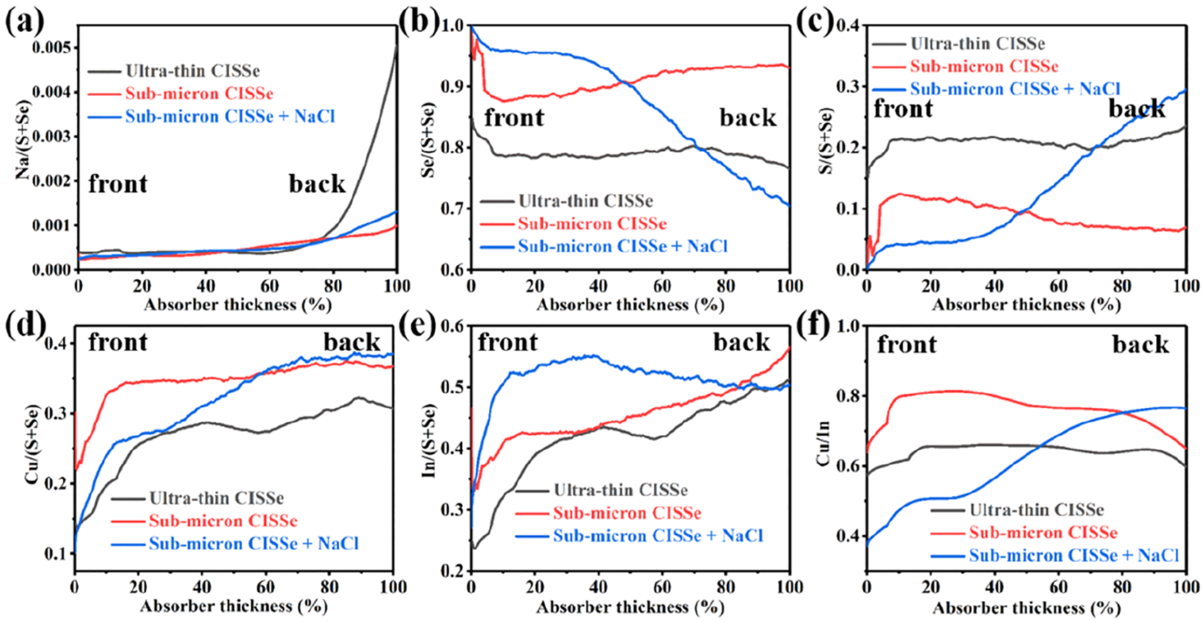

Figure 6. Composition details of ultrathin (550 nm) and submicron (740 nm) CISSe absorber films without and with NaCl treatment measured by GDOES: (a) Na/(S + Se), (b) Se/(S + Se), (c) S/(S + Se), (d) Cu/(S + Se), (e) In/(S + Se), and (f) Cu/In ratios. The absorber thicknesses are normalized to 100% (corresponding to the absorber). The selenization was carried out at T = 520 °C.

3.2. Effect of Absorber Thickness and NaCl Treatment. The absorber thickness can strongly affect the solar cell properties.[9] Thinner absorber layers result in low cost because they reduce material consumption and increase production throughput. However, the efficiency of thin absorbers is limited by electrical and optical losses, such as increased recombination at back contact and reduced light absorption.[3−6,29] As shown in the previous section, the best solar cell properties are obtained for absorbers selenized at 520 °C, thus T = 520 °C will be used for exploring the effect of absorber thickness. Three absorber thicknesses are utilized for the investigations: 550 nm (ultrathin absorber), 740 nm (submicron absorber), and 1440 nm (micron absorber). The best device with a submicron CISSe absorber exhibits an efficiency of 7.9%, which is 0.4% (abs.) higher than that of the ultrathin CISSe device (Figure 5a). However, ultrathin CISSe shows a higher V_{oc} of 481.7 mV compared to 445.6 mV for the submicron CISSe, whereas the opposite trend is observed for j_{sc} and FF. Previous reports have proven that the fabrication of thick absorbers via a solution process will lead to carbon residuals and voids at the interface between the absorber and the back contact.[8,30] These defects located at the rear interface will increase the recombination and result in a lower V_{oc}. The increase in j_{sc} of submicron solar cells can be attributed to higher light absorption due to the thicker absorber. CISSe solar cells with a micron absorber show inferior properties and poor uniformity; the highest PCE of these devices is 1.8% (Figure S4). . V_{oc}, j_{sc}, and FF are significantly reduced to 376.0 mV, 16.4 mA/cm^2, and 29.8%, respectively. The absorbers easily peel off from the ITO back contact in this case. The series resistance decreases from 2.2 Ω cm^2 for the ultrathin absorber to 1.1 Ω cm^2 for the submicron absorber (Figure S5 and Table 2). As the adhesion to the ITO back contact may become a challenge for thick absorbers and the best efficiency of CISSe solar cells on ITO was obtained for submicron absorbers, these are utilized for further research.

Indeed, compared to ultrathin absorbers, increasing the absorber thickness to submicron (740 nm) can improve the CISSe solar cell properties. However, a lower V_{oc} is obtained for the thicker absorbers. It is known that Na incorporation can significantly increase the V_{oc} of CIGSe-based solar cells.[20,26] The J-V results of submicron CISSe subject to a preselenization treatment with various concentrations of NaCl solution are shown in Figure S6 and Table S3. The corresponding electrical properties are shown in Figure S7. The efficiency increases to 8.0% using 1 M NaCl for preselenization treatment (Figure 5a). Additionally, the V_{oc} increases to a value of 466.0 mV; however, the j_{sc} and FF slightly decrease to 28.7 mA/cm^2 and 59.6%, respectively. For the respective best-performing devices, the reference CISSe solar cell presents a higher j_{sc} and FF than the CISSe solar cells subject to Na treatment at various concentrations (Figure S6). Furthermore, the j_{sc} and FF of the best-performing CISSe solar cells

https://doi.org/10.1021/acsaem.2c01764
ACS Appl. Energy Mater. 2022, 5, 12252−12260

incorporating Na decrease with increasing Na concentration before starting to recover (for 1 M NaCl).

The reference ultrathin CISSe solar cell presents an EQE peaking at 74% for 540 nm wavelength. For the submicron CISSe solar cell, the EQE also peaks at 540 nm with a value surpassing 87%. The highest EQE is observed in the range from 380 to 1300 nm wavelength for submicron CISSe solar cells. The submicron CISSe solar cell with 1 M NaCl treatment has a higher EQE photoresponse. A narrower band gap of the submicron CISSe solar cells (both with or without NaCl treatment) can be calculated from the EQE spectrum according to the formula $[E \times \ln(1 - \mathrm{EQE})]^2$.

Compared to the ultrathin CISSe device, both the N_{cv} and W_d of submicron CISSe decrease. The submicron CISSe without NaCl treatment has a charge carrier density of 1.9×10^{16} cm^{-3} and a W_d of 315.0 nm. The absorber with 1 M NaCl treatment exhibits a lower hole density (9.1×10^{15} cm^{-3}) and the W_d decreases to 303.5 nm. The remarkable lower hole density should be attributed to higher recombination at the rear interface, reducing V_{oc} and PCE.[7]

4. DISCUSSION

4.1. Effect of Absorber Thickness. Ultrathin (550 nm) and submicron (740 nm) CISSe absorbers have a similar content of Cu and In per unit thickness because these elements originate from the precursor solution and they will not volatilize seriously during the selenization process. Elemental S will volatilize during the selenization and be replaced by Se. All precursor films are subject to a selenization process utilizing the same content of Se. Therefore, the content of Se in various absorber thicknesses is different per unit thickness. In other words, the thin absorber has a higher Se/(total elements) ratio.

A higher Na/(S + Se) ratio exists near the rear interface of the ultrathin absorber as compared to the submicron absorber (Figure 6a). The possible reason is that while the same amount of Na diffuses into the absorber from the glass substrate during the high-temperature selenization process, the thinner absorber obtains a higher Na content per unit thickness. The submicron absorber has a higher Se/(S + Se), Cu/(S + Se), and In/(S + Se) ratio compared to the ultrathin absorber (Figure 6b-e). These results can be explained by the formation of a dense large-grained layer at the front surface of the ultrathin absorber.[13] It is reported that Na can promote the transformation of fine grains into large ones during selenization. The ultrathin absorber has a shorter diffusion distance of Na than the submicron absorber. Therefore, it is expected that the formation of a dense layer with large grains is facilitated in the ultrathin absorber. This dense layer will inhibit the diffusion of Se toward the absorber and limit the volatilization of S.[13,31] Thus, the result is that the ultrathin absorber has a larger Se/(Se + S) than that of the submicron absorber. A higher Se/(S + Se) ratio is still observed at the front surface owing to the large-grained layer at near-surface (Figure 6b).[13] Correspondingly, the S/(S + Se) content is lower at the front surface and increases toward the back. As stated before, both ultrathin and submicron precursor films are selenized in the same content of Se, so the ultrathin absorbers have an overall higher content of Se/(S + Se). As Cu and In are introduced through the precursor solution and, therefore, have similar concentrations, the ultrathin absorbers have an overall lower Cu/(S + Se) and In/(S + Se) ratio than submicron absorbers. Both absorber types present a consistent tendency of Cu/In with higher Cu/In ratios in the bulk and lower at the front and rear interface. This increase in Cu/In ratios toward the bulk can be explained by forming a Cu-poor layer at the front interface [potential combination of $CuIn(S,Se)_2$ and $CuIn_3(S,Se)_5$]. The decrease of Cu/In ratios at the rear interface can be ascribed to a small content of In loss owing to the formation of $In_2(S_x,Se_{1-x})_3$ during the selenization.[24]

4.2. Effect of NaCl Treatment. Generally, the ultrathin and submicron absorbers have a similar Na/(S + Se) ratio at the front surface because the excess Na is removed by a KCN etching process (Figure 6a).[32,33] However, NaCl preselenization treatment will result in a redistribution of elements (Figure S8). Compared to the absorbers without NaCl treatment, the addition of Na results in a smaller value of Cu/(S + Se) (Figure 6d) and a larger value of In/(S + Se) (Figure 6e), leading to a smaller Cu/In ratio (Figure 6f). The Cu/In ratio near the surface of the submicron CISSe absorbers with a NaCl preselenization treatment is 0.37 only (Figure 6f), which can be explained by the formation of the copper-deficient ordered vacancy compound $CuIn_3Se_5$ [the ratio of Se/(Se + S) is close to 100% at near-surface in Figure 6b].[32−34] This Cu-poor compound between the absorber and buffer layer can improve the CISSe solar cell performance, including a higher efficiency. When the absorber is subject to NaCl preselenization treatment, Na can bond with Se to form Na_2Se_x which is beneficial for the formation of a dense layer of large grains at the absorber surface, inhibiting the diffusion of elemental Se toward the absorber and limiting the volatilization of S.[8,13,32,33] Therefore, the absorber with NaCl preselenization treatment has a high Se/(S + Se) at the very front surface of the absorber and an overall inverse composition profile of S/(S + Se) (Figure 6b,c).

5. CONCLUSIONS

Ultrathin and submicron CISSe solar cells are successfully fabricated on ITO back contact via a low-cost metal-chloride DMF solution process. Variations of selenization temperature are investigated. Increasing the selenization temperature above 520 °C may improve the crystallinity, morphology, and homogeneity of the CISSe absorbers. We demonstrate that 7.5% efficiency for semitransparent ultrathin CISSe solar cells (550 nm CISSe absorber thickness) is obtained at 520 °C of selenization. So far, to the best of our knowledge, our results have achieved the highest performance for ultrathin CISSe solar cells grown on ITO back contact via a solution process (Table S4). Furthermore, CISSe solar cells with different absorber thicknesses are studied. The efficiency of these solar cells first increases with the absorber thickness increasing to submicron (740 nm); however, it decreases when reaching micron (1440 nm) thickness. In addition, CISSe solar cells can achieve an efficiency of 8% when the submicron absorber is subject to 1 M NaCl solution treatment. This work offers a facile method to prepare high-quality Na-doped CISSe films for integration in semitransparent solar cell devices.

■ ASSOCIATED CONTENT

Supporting Information

The Supporting Information is available free of charge at https://pubs.acs.org/doi/10.1021/acsaem.2c01764.

Sheet resistance and optical properties of annealed ITO; XRF results; optical properties and series resistances of ultrathin CISSe absorbers; J−V curve of the micron CISSe device; series resistance; PV parameters of NaCl treatment CISSe; fitting electrical parameters; S/(S + Se) ratios of NaCl treatment CISSe absorbers; and overview on high-performance TCO/CIGSSe-based solar cells (PDF)

AUTHOR INFORMATION

Corresponding Authors

Guanchao Yin − *School of Materials Science and Engineering, Wuhan University of Technology, 430070 Wuhan, China;* orcid.org/0000-0002-4389-605X; Email: guanchao.yin@whut.edu.cn

Martina Schmid − *CENIDE, Faculty of Physics, University of Duisburg-Essen, 47057 Duisburg, Germany;* orcid.org/0000-0001-5103-0750; Email: martina.schmid@uni-due.de

Authors

Yao Gao − *CENIDE, Faculty of Physics, University of Duisburg-Essen, 47057 Duisburg, Germany*

Yong Li − *CENIDE, Faculty of Physics, University of Duisburg-Essen, 47057 Duisburg, Germany*

Tristan Köhler − *CENIDE, Faculty of Physics, University of Duisburg-Essen, 47057 Duisburg, Germany*

Jan Lucaßen − *CENIDE, Faculty of Physics, University of Duisburg-Essen, 47057 Duisburg, Germany*

Complete contact information is available at: https://pubs.acs.org/10.1021/acsaem.2c01764

Notes

The authors declare no competing financial interest.

ACKNOWLEDGMENTS

The authors would like to thank Klaus Pärschke for the window layer and front contact deposition. The authors would also like to thank Alexander Poßberg, AG Weimann (UDE), for support with XRD measurements and AG Winterer (UDE) for the discussion. The XRF and GDOES measurements were performed on an instrument funded by the Deutsche Forschungsgemeinschaft (DFG, German Research Foundation)-INST 20876/324-1 FUGG and are acknowledged as follows: "Gefördert durch die Deutsche Forschungsgemeinschaft (DFG)-Projektnummer INST 20876/324-1 FUGG". Y.G. and Y.L. specially acknowledge the financial support of the Chinese Scholarship Committee, and Y.L. acknowledges the funding from the University of Duisburg-Essen graduation grant. G.Y. acknowledges the funding from the National Natural Science Foundation of China (NSFC, 51802240).

REFERENCES

(1) Nakamura, M.; Yamaguchi, K.; Kimoto, Y.; Yasaki, Y.; Kato, T.; Sugimoto, H. Cd-Free Cu(In,Ga)(Se,S)$_2$ Thin-Film Solar Cell With Record Efficiency of 23.35. *IEEE J. Photovoltaics* **2019**, *9*, 1863−1867.

(2) Ramanujam, J.; Singh, U. P. Copper Indium Gallium Selenide Based Solar Cells - a Review. *Energy Environ. Sci.* **2017**, *10*, 1306−1319.

(3) Yin, G.; Brackmann, V.; Hoffmann, V.; Schmid, M. Enhanced Performance of Ultra-thin Cu(In,Ga)Se$_2$ Solar Cells Deposited at Low Process Temperature. *Sol. Energy Mater. Sol. Cells* **2015**, *132*, 142−147.

(4) van Lare, C.; Yin, G.; Polman, A.; Schmid, M. Light Coupling and Trapping in Ultrathin Cu(In,Ga)Se$_2$ Solar Cells Using Dielectric Scattering Patterns. *ACS Nano* **2015**, *9*, 9603−9613.

(5) Yin, G.; Knight, M. W.; van Lare, M. C.; Solà Garcia, M. M.; Polman, A.; Schmid, M. Optoelectronic Enhancement of Ultrathin CuIn$_{1-x}$Ga$_x$Se$_2$ Solar Cells by Nanophotonic Contacts. *Adv. Opt. Mater.* **2017**, *5*, 1600637.

(6) Yin, G.; Song, M.; Schmid, M. Rear Point Contact Structures for Performance Enhancement of Semi-transparent Ultrathin Cu(In,Ga)-Se$_2$ Solar Cells. *Sol. Energy Mater. Sol. Cells* **2019**, *195*, 318−322.

(7) Li, Y.; Yin, G.; Gao, Y.; Köhler, T.; Lucaßen, J.; Schmid, M. Sodium Control in Ultrathin Cu(In,Ga)Se$_2$ Solar Cells on Transparent Back Contact for Efficiencies Beyond 12%. *Sol. Energy Mater. Sol. Cells* **2021**, *223*, 110969.

(8) Jiang, J.; Yu, S.; Gong, Y.; Yan, W.; Zhang, R.; Liu, S.; Huang, W.; Xin, H. 10.3% Efficient CuIn(S,Se)$_2$ Solar Cells from DMF Molecular Solution with the Absorber Selenized under High Argon Pressure. *Sol. RRL* **2018**, *2*, 1800044.

(9) Shin, M. J.; Park, S.; Lee, A.; Park, S. J.; Cho, A.; Kim, K.; Ahn, S. K.; Hyung Park, J. H.; Yoo, J.; Shin, D.; Jeong, I.; Yun, J. H.; Gwak, J.; Cho, J. Bifacial Photovoltaic Performance of Semitransparent Ultrathin Cu(In,Ga)Se$_2$ Solar Cells with Front and Rear Transparent Conducting Oxide Contacts. *Appl. Surf. Sci.* **2021**, *535*, 147732.

(10) Son, Y.-S.; Yu, H.; Park, J.-K.; Kim, W. M.; Ahn, S.-Y.; Choi, W.; Kim, D.; Jeong, J. Control of Structural and Electrical Properties of Indium Tin Oxide (ITO)/Cu(In,Ga)Se$_2$ Interface for Transparent Back-Contact Applications. *J. Phys. Chem. C* **2019**, *123*, 1635−1644.

(11) Chantana, J.; Arai, H.; Minemoto, T. Trap-Assisted Recombination for Ohmic-Like Contact at P-type Cu(In,Ga)Se$_2$/Back N-type TCO Interface in Superstrate-Type Solar Cell. *J. Appl. Phys.* **2016**, *120*, 045302.

(12) Zhang, T.; Yang, Y.; Liu, D.; Tse, S. C.; Cao, W.; Feng, Z.; Chen, S.; Qian, L. High Efficiency Solution-Processed Thin-Film Cu(In,Ga)(Se,S)$_2$ Solar Cells. *Energy Environ. Sci.* **2016**, *9*, 3674−3681.

(13) Jiang, J.; Giridharagopal, R.; Jedlicka, E.; Sun, K.; Yu, S.; Wu, S.; Gong, Y.; Yan, W.; Ginger, D. S.; Green, M. A.; Hao, X.; Huang, W.; Xin, H. Highly Efficient Copper-Rich Chalcopyrite Solar Cells from DMF Molecular Solution. *Nano Energy* **2020**, *69*, 104438.

(14) Clark, J. A.; Murray, A.; Lee, J. M.; Autrey, T. S.; Collord, A. D.; Hillhouse, H. W. Complexation Chemistry in N,N-Dimethylformamide-Based Molecular Inks for Chalcogenide Semiconductors and Photovoltaic Devices. *J. Am. Chem. Soc.* **2019**, *141*, 298−308.

(15) Suresh, S.; Uhl, A. R. Present Status of Solution-Processing Routes for Cu(In,Ga)(S,Se)$_2$ Solar Cell Absorber. *Adv. Energy Mater.* **2021**, *11*, 2003743.

(16) Romanyuk, Y. E.; Hagendorfer, H.; Stücheli, P.; Fuchs, P.; Uhl, A. R.; Sutter-Fella, C. M.; Werner, M.; Haass, S.; Stückelberger, J.; Broussillou, C.; Grand, P.-P.; Bermudez, V.; Tiwari, A. N. All Solution-Processed Chalcogenide Solar Cells-From Single Functional Layers Towards a 13.8% Efficient CIGS Device. *Adv. Funct. Mater.* **2015**, *25*, 12−27.

(17) Barange, N.; Chu, V. B.; Nam, M.; Ahn, I. H.; Kim, Y. D.; Han, I. K.; Min, B. K.; Ko, D. H. Ordered Nanoscale Heterojunction Architecture for Enhanced Solution-Based CuInGaS$_2$ Thin Film Solar Cell Performance. *Adv. Energy Mater.* **2016**, *6*, 1601114.

(18) Sousa, V.; Goncalves, B. F.; Rosen, Y. S.; Virtuoso, J.; Anacleto, P.; Cerqueira, M. F.; Modin, E.; Alpuim, P.; Lebedev, O. I.; Magdassi, S.; Sadewasser, S.; Kolen'ko, Y. V. Over 6% Efficient Cu(In,Ga)Se$_2$ Solar Cell Screen-Printed from Oxides on Fluorine-Doped Tin Oxide. *ACS Appl. Energy Mater.* **2020**, 3, 3120−3126.

(19) Gouillart, L.; Cattoni, A.; Goffard, J.; Donsanti, F.; Patriarche, G.; Jubault, M.; Naghavi, N.; Collin, S. Development of Reflective Back Contacts for High-Efficiency Ultrathin Cu(In,Ga)Se$_2$ Solar Cells. *Thin Solid Films* **2019**, *672*, 1−6.

(20) Guo, Q.; Ford, G. M.; Agrawal, R.; Hillhouse, H. W. Ink Formulation and Low-Temperature Incorporation of Sodium to Yield 12% Efficient Cu(In,Ga)(S,Se)$_2$ Solar Cells from Sulfide Nanocrystal Inks. *Prog. Photovoltaics Res. Appl.* **2013**, *21*, 64−71.

(21) Gao, Y.; Wang, J.; Mo, S.; Wang, F.; Long, F.; Zou, Z. Synthesis of High-Quality Wurtzite Cu$_2$ZnSn(S$_{1-x}$,Se$_x$)$_4$ Nanocrystals With Non-Toxic Selenium Precursor and the Photoelectrochemical Performance of ZnO NAs/CZTSSe Heterojunction. *Sol. RRL* **2018**, *2*, 1800015.

(22) Yuan, Z.-K.; Chen, S.; Xie, Y.; Park, J.-S.; Xiang, H.; Gong, X.-G.; Wei, S.-H. Na-Diffusion Enhanced P-type Conductivity in Cu(In,Ga)Se_2: A New Mechanism for Efficient Doping in Semiconductors. *Adv. Energy Mater.* **2016**, *6*, 1601191.

(23) Zeng, L.; Zeng, C.; Liang, Y.; Yuan, Y.; Yan, G.; Hong, R. Significant Passivation Effect of Cu(In,Ga)Se_2 Solar Cells via Back Contact Surface Modification Using Oxygen Plasma. *Sol. RRL* **2021**, *5*, 2000572.

(24) Chantana, J.; Nishimura, T.; Kawano, Y.; Suyama, N.; Yamada, A.; Kimoto, Y.; Kato, T.; Sugimoto, H.; Minemoto, T. Aging Effect of a Cu(In,Ga)$(S,Se)_2$ Absorber on the Photovoltaic Performance of Its Cd-Free Solar Cell Fabricated by an All-Dry Process: Its Carrier Recombination Analysis. *Adv. Energy Mater.* **2019**, *9*, 1902869.

(25) Halim, M. A.; Islam, M. M.; Luo, X.; Sakurai, T.; Sakai, N.; Kato, T.; Sugimoto, H.; Tampo, H.; Shibata, H.; Niki, S.; Akimoto, K. A Comparative Study on Charge Carrier Recombination Across the Junction Region of $Cu_2ZnSn(S,Se)_4$ and Cu(In,Ga)Se_2 Thin Film Solar Cells. *AIP Adv.* **2016**, *6*, 035216.

(26) Uličná, S.; Welch, L. M.; Abbas, A.; Togay, M.; Tsai, V.; Betts, T. R.; Malkov, A. V.; Walls, J. M.; Bowers, J. W. Sodium Doping of Solution-Processed Amine-Thiol Based CIGS Solar Cells by Thermal Evaporation of NaCl. *Prog. Photovoltaics Res. Appl.* **2021**, *29*, 546−557.

(27) Chantana, J.; Kawano, Y.; Nishimura, T.; Kimoto, Y.; Kato, T.; Sugimoto, H.; Minemoto, T. Effect of Alkali Treatment on Photovoltaic Performances of Cu(In,Ga)$(S,Se)_2$ Solar Cells and Their Absorber Quality Analyzed by Urbach Energy and Carrier Recombination Rates. *ACS Appl. Energy Mater.* **2020**, *3*, 1292−1297.

(28) Chantana, J.; Nishimura, T.; Kawano, Y.; Teraji, S.; Watanabe, T.; Minemoto, T. Examination of Relationship between Urbach Energy and Open-Circuit Voltage Deficit of Flexible Cu(In,Ga)Se_2 Solar Cell for Its Improved Photovoltaic Performance. *ACS Appl. Energy Mater.* **2019**, *2*, 7843−7849.

(29) Kong, Y.; Huang, L.; Chi, Z.; Wu, X.; Li, J.; Xiao, X. Failure and Recovery Modes of Submicron Cu(In,Ga)Se_2 Solar Cells with High Cu Content. *ACS Appl. Mater. Interfaces* **2020**, *12*, 52857−52863.

(30) Lin, X.; Klenk, R.; Wang, L.; Koehler, T.; Albert, J.; Fiechter, S.; Ennaoui, A.; Lux-Steiner, M. 11.3% Efficiency Cu(In,Ga)$(S,Se)_2$ Thin Film Solar Cells via Drop-on-Demand Inkjet Printing. *Energy Environ. Sci.* **2016**, *9*, 2037−2043.

(31) Keller, J.; Bilousov, O. V.; Neerken, J.; Wallin, E.; Martin, N. M.; Riekehr, L.; Edoff, M.; Platzer-Björkman, C. Heavy Alkali Treatment of Post-Sulfurized Cu(In,Ga)Se_2 Layers: Effect on Absorber Properties and Solar Cell Performance. *Sol. RRL* **2020**, *4*, 2000248.

(32) Colombara, D.; Werner, F.; Schwarz, T.; Cañero Infante, I.; Fleming, Y.; Valle, N.; Spindler, C.; Vacchieri, E.; Rey, G.; Guennou, M.; Bouttemy, M.; Manjón, A. G.; Peral Alonso, I.; Melchiorre, M.; El Adib, B.; Gault, B.; Raabe, D.; Dale, P. J.; Siebentritt, S. Sodium Enhances Indium-Gallium Interdiffusion in Copper Indium Gallium Diselenide Photovoltaic Absorbers. *Nat. Commun.* **2018**, *9*, 826.

(33) Berner, U.; Colombara, D.; De Wild, J.; Robert, E. V. C.; Schütze, M.; Hergert, F.; Valle, N.; Widenmeyer, M.; Dale, P. J. 13.3% Efficient Solution Deposited Cu(In,Ga)Se_2 Solar Cells Processed with Different Sodium Salt Sources. *Prog. Photovoltaics Res. Appl.* **2016**, *24*, 749−759.

(34) Hofmann, A.; Pettenkofer, C. The $CuInSe_2$-$CuIn_3Se_5$ Defect Compound Interface: Electronic Structure and Band Alignment. *Appl. Phys. Lett.* **2012**, *101*, 062108.

https://doi.org/10.1021/acsaem.2c01764
ACS Appl. Energy Mater. 2022, 5, 12252−12260